Dual seismic migration velocities in seismic swarms

Pierre Dublanchet, Louis De Barros

AGU ADVANCING EARTH AND SPACE SCIENCE

Geophysical Research Letters

RESEARCH LETTER
10.1029/2020GL090025

Dual Seismic Migration Velocities in Seismic Swarms

P. Dublanchet[1] and L. De Barros[2]

[1]MINES ParisTech, PSL Research University, Centre de Géosciences, Fontainebleau, France, [2]Université Côte d'Azur, CNRS, OCA, IRD, Géoazur, Sophia Antipolis, Valbonne, France

Key Points:

- We propose a new model for fluid-driven earthquake migration coupling fluid diffusion aseismic slip and earthquakes
- The dual seismic migration pattern observed in a Corinth rift swarm is reproduced by our model
- Migration speeds are controlled by the rate of increase of mean pore pressure and state of initial stress and not by hydraulic diffusivity

Supporting Information:

- Supporting information S1

Correspondence to:

P. Dublanchet,
pierre.dublanchet@mines-paristech.fr

Citation:

Dublanchet, P., & De Barros, L. (2020). Dual seismic migration velocities in seismic swarms. *Geophysical Research Letters*, *47*, e2020GL090025. https://doi.org/10.1029/2020GL090025

Received 23 JUL 2020
Accepted 20 NOV 2020

Abstract Fluid-induced earthquake sequences generally appear as expanding swarms activating a particular fault. The recent analysis of a swarm in the Corinth rift has revealed a dual migration pattern, with a global slow expansion (m day^{-1}) and episodes of rapid migration (km day^{-1}). Such swarms are generally interpreted as fluid diffusion, which ignores the possibility of static, dynamic, or aseismic triggering and the existence of rapid migration. Here, we propose a new model for such swarms, where earthquakes consist in the failure of asperities on a creeping fault infiltrated by fluid. For that, we couple rate-and-state friction, nonlinear diffusivity, and elasticity along a 1D interface. This model reproduces the dual migration speeds observed in real swarms. We show that migration speeds increase linearly with the mean pressurization and are not dependent on the hydraulic diffusivity, as traditionally suggested.

Plain Language Summary The common interpretation of earthquake swarms assumes a fluid diffusion from a source at depth, which destabilizes critically stressed faults. In this model, seismicity is localized at the fluid front. However, earthquake swarms expand faster than fluid is likely to diffuse. Recent observations in the Corinth rift (Greece) also report that swarms consist in the succession of bursts of rapidly migrating events, which is not explained by the diffusion model. To account for these features, one needs to consider slow slip on faults (undetected at the surface) in addition to fluid diffusion. Here, we propose a physics-based model coupling fluid diffusion, slow slip, and earthquake triggering on a 1D fault. Our model reproduces the dual migration (slow expansion and rapid bursts) pattern of some seismic swarms. We also show that migration speeds are controlled by the increase of the mean pore pressure within the fault and not by hydraulic diffusivity.

1. Introduction

Seismic swarms are sequences of earthquakes, clustered in time and space, where no mainshock could be identified. To ensure such an activity during days to months, a driving mechanism is required. It could be pressure diffusion, as such swarms are induced by reservoir (injection and impoundment) activities (Deichmann & Giardini, 2009; Diehl et al., 2017; Dinske et al., 2010; Ellsworth, 2013; Lengliné et al., 2017). The similarity between induced and natural swarms suggests that even natural swarms are driven by transient episodes of fluid flow at depth. This conclusion is generally supported by the diffusive character of the swarms expansion. The classical model involves the diffusion of a fluid from a source at depth, leading to pore pressure and thus effective normal stress variations on critically prestressed faults bringing them to seismic failure (Shapiro & Dinske, 2009). In this model, the swarm expansion exactly tracks the fluid front at depth and could be used to estimate the hydraulic diffusivity of the swarm region. This generally leads to diffusivity estimates varying between 0.001 and 1 m^2 s^{-1} (Duverger et al., 2015; Goertz-Allmann et al., 2017; Hainzl & Fischer, 2002; Hainzl et al., 2012; Lengliné et al., 2017; Schoenball & Ellsworth, 2017; Shapiro & Dinske, 2009), which is orders of magnitude larger than in situ measurements of fault hydraulic properties (Doan et al., 2006). Furthermore, it does not account for static and dynamic triggering, which could eventually trigger seismicity beyond the fluid front.

Recent in situ fault slip reactivation experiments (Duboeuf et al., 2017;Guglielmi et al., 2015) and seismological observations (Bourouis & Bernard, 2007; Cauchie et al., 2020; De Barros et al., 2020; Eyre et al., 2019, 2020; Hatch et al., 2020; Lengliné et al., 2017; Lohman & McGuire, 2007; Wei et al., 2015) have revealed that significant slow (aseismic) slip has to be taken into account in the triggering of fluid-induced seismicity. In this alternative model, the pore pressure changes trigger an aseismic slip front propagating on faults,

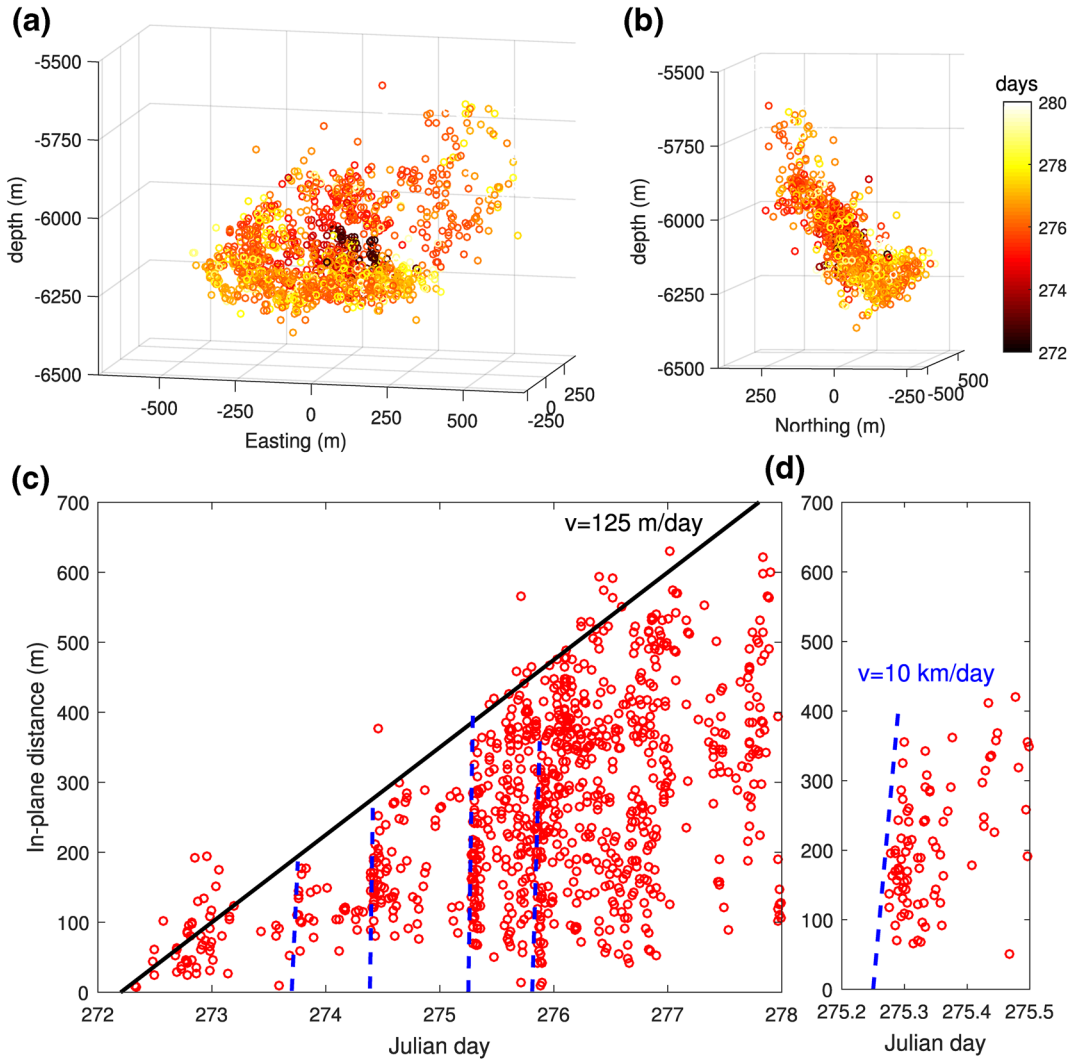

Figure 1. Location and migration of the seismicity during the 2015 Corinth gulf swarm (De Barros et al., 2020). (a**)** 3D location of the seismicity, view from South. Colorscale shows the days of occurrence. (b**)** Same as (a), with a view from West. (c) Distance versus time (*R*–*T* plot) for the first 6 days of swarm activity. The position of reference is the mean position of the first 10 events. The black line shows the overall migration of the swarm (125 m day^{-1}), while the dashed blue lines highlight episodes of fast migration velocities. The gray areas show the spatiotemporal density of events. (d) Same as (c), zoomed on a fast migration period.

leading to the failure of preexisting asperities (earthquakes). Aseismic slip fronts are known to propagate at speeds of the order of km day^{-1} (Lohman & McGuire, 2007; Obara, 2010; Radiguet et al., 2011; Rubin & Armbruster, 2013), which is in agreement with fast-velocity migration observed during some swarms (Lohman & McGuire, 2007).

A recent analysis of an earthquake swarm occurring in the Corinth rift (Greece) has revealed a particular migration pattern shown in Figure 1 (De Barros et al., 2020). It consists of a slow (125 m day^{-1}) expansion of the swarm, involving several episodes of rapid (~10 km day^{-1}) earthquake migrations. This swarm could therefore be seen as an intermittent growth involving a succession of rapidly migrating earthquake bursts, penetrating each time further on the fault. Such patterns with dual behaviors seem to characterize other swarms of natural origin, such as in the Corinth rift (Bourouis & Cornet, 2009; Duverger et al., 2015), in western Bohemia (Hainzl & Fischer, 2002; Hainzl et al., 2012), in Nevada (Hatch et al., 2020), and induced by reservoir operations (Bourouis & Bernard, 2007; Cauchie et al., 2020; Diehl et al., 2017; Eyre et al., 2019; Lengliné et al., 2017). Here again, the simple model of triggering by fluid diffusion fails to explain the

episodes of rapid earthquake migration occurring within the swarm once the fluid front passed. An additional process is therefore needed. Coulomb stress transfer from earthquakes may lead to cascading seismicity on near critical faults, as suggested by Schoenball and Ellsworth (2017) to explain the Oklahoma seismicity. Such migration velocity differences may also be related to highly heterogeneous or slip-enhanced permeability, but this is not likely to lead to a factor of 100 difference in the migration velocity. Slow, aseismic slip is a likely candidate to explain these dual behaviors, as the overall expansion may be associated with fluid diffusion while fast migration may suggest slow slip triggering on particular asperities.

Recent modeling efforts have shown that fluid-induced aseismic slip fronts propagate faster that pore pressure diffusion on frictional faults (Cappa et al., 2019; Bhattacharya & Viesca, 2019; Dublanchet, 2019; Wynants-Morel et al., 2020) and that earthquake location tracks the stress perturbation associated with the aseismic slip front. These studies have also demonstrated the importance of permeability enhancement related to slip in this triggering process. However, none of these models reproduce the dual migration of earthquakes. One of the reason is that these approaches do not produce repeating earthquakes, because either purely strengthening or slip weakening friction is used.

Here, we propose a new modeling approach aiming at better constraining the processes that drive the swarm seismicity, by looking for the physical parameters leading to the dual migration observed in the Corinth rift swarm (Figure 1). The model assumes nonlinear fluid diffusion within a heterogeneous rate-and-state frictional interface between elastic solids. Thanks to rate-and-state friction, the fault is able to produce aseismic slip and to generate earthquake cycles. The nonlinearity of pore pressure diffusion comes from a permeability evolution that accounts for the past slip history on the fault. The next section is dedicated to a description of the model. Then, different hydraulic scenarios are tested, and we demonstrate which parameters principally control the dual migration velocities.

2. Model

Because of the radial migration pattern of the Corinth swarm (Figure 1), we model a tectonic fault as a 1D linear interface of length L between two elastic slabs of thickness H (Figure S1). The fault is loaded by a constant lithostatic normal stress σ, and a constant slip rate $\pm\, v_0/2$ at the top and bottom limits of the slabs so that slip occurs in mode III along the fault. Based on the Corinth swarm in Figure 1, we choose $L = 1.2$ km and $\sigma = 153$ MPa (~6 km depth with a rock density of ~2,600 kg m^{-3}). We also used $H = 3$ km and $v_0 = 4.825$ mm year^{-1} in order to reproduce the interseismic strain rate of 10^{-7} year^{-1} in the Corinth rift in the absence of fault slip (Bernard et al., 2006). We note x the along fault distance, t the time, and $\delta(x, t)$ the relative slip. The interface obeys rate-and-state friction (Dieterich, 1979; Ruina, 1983) where the friction coefficient f depends on the slip rate $v(x,t) = \dot{\delta}$ and a state variable $\theta(x, t)$ accounting for the past slip history of the interface. f is given by

$$f = f_0 + a \ln \frac{v}{v_0} + b \ln \frac{\theta v_0}{d_c}, \tag{1}$$

where f_0, a, b, and d_c are a constant friction coefficient, nondimensional rate-and-state parameters, and a critical slip distance, respectively. We assume standard laboratory values for $d_c = 0.0153$ mm and $f_0 = 0.6$ (Marone, 1998). From Ruina (1983), we assume that θ evolves according to the aging law:

$$\dot{\theta} = 1 - \frac{v\theta}{d_c}. \tag{2}$$

Recall that if $\dot{\theta} = 0$, the friction is at steady state, and the friction coefficient only depends on slip rate: $f = f_{ss}(v)$, where

$$f = f_0 + (a - b) \ln \frac{v}{v_0}. \tag{3}$$

In order to account for possible aseismic slip and earthquakes, we consider a heterogeneous distribution of the $a - b$ parameter. Seismogenic asperities are modeled as critical velocity-weakening patches ($a - b < 0$, larger than the critical nucleation length [Rubin & Ampuero, 2005]) distributed on a velocity-strengthening

region $a - b > 0$. We achieve this by using a constant value of $b = 0.001$, and a variable a parameter, with $a = 0.1b$ on seismogenic asperities and $a = 1.35b$ on creeping regions. Asperities are 9 m long and separated by 21 m.

We assume a fluid flowing exclusively within the fault under the pore pressure $p(x, t)$, so that the frictional stress τ_f writes:

$$\tau_f = f(\sigma - p). \tag{4}$$

From Darcy's law and fluid mass balance, pore pressure evolution is controlled by the following nonlinear diffusion equation:

$$\frac{\partial p}{\partial t} = \frac{\partial}{\partial x}\left[D\frac{\partial p}{\partial x} \right] + q, \tag{5}$$

where $D(x, t)$ is the space-dependent and time-dependent hydraulic diffusivity. $q(x, t)$ is the source term, modeling the injection at the center of the fault, as suggested by the migration of Corinth earthquakes (Figure 1). We define the mean pressurization of the fault Π_m (in Pa.s^{-1}) as:

$$q(x,t) = L\Pi_m \delta_D(x), \tag{6}$$

where δ_D is the Dirac delta function and L is the fault length. When taking the spatial average of Equation 5, Π_m is the rate of mean pressure increase in the fault. Note that Π_m is not the pore pressure rate at the injection point p_0, but under a constant diffusivity assumption, we have at time t (Dublanchet, 2019):

$$p_0 = \frac{\Pi_m L}{\sqrt{\pi D}}\sqrt{t}, \tag{7}$$

We derive in the supporting information, a relationship between diffusivity D and state variable θ of the form:

$$D = D_0 e^{-\theta/\tau_v}, \tag{8}$$

where D_0 is a constant reference diffusivity, and $\tau_v = \eta/2\sigma_Y$ is a viscoelastic relaxation time characterizing the microasperities of the interface (η being the effective viscosity of the rock material, and σ_Y the yield stress, taken for simplicity as the shear modulus of the rock $\mu = 30$ GPa). The derivation is based on the interpretation of the state variable θ as a measure of the age of microasperities (Ruina, 1983). Equation 8 leads to a slip history dependence of D. When the fault is locked (v is negligible), θ increases linearly with time according to the aging law (2), and D decreases exponentially. Similarly, during fast slip, θ decreases leading to diffusivity enhancement. The maximum possible value of D is approximately D_0, and the minimum value of the order of $D_0 e^{-5/\tau_v} = 10^{-11} D_0$, assuming a maximum state variable of 5 and $\tau_v = 0.23$ days. Diffusivity variations are also illustrated in Figures S5, S9, S13, and S14.

The frictional stress is balanced by the quasi-dynamic elastic stress $\tau_e(x, t)$ given by:

$$\tau_e = -\mathcal{K} * (\delta - v_0 t) - \eta_D v \tag{9}$$

where $\mathcal{K}$ is the elastic kernel derived by Horowitz and Ruina (1989). η_D is the radiation damping (Rice, 1993) given by $\eta_D = \mu/2c_s$, where μ is the shear modulus and c_s the shear-wave speed ($c_s = 3.4$ km s^{-1}). The star denotes spatial convolution. The first term on the right side of Equation 9 corresponds to the stress redistribution associated with slip along the interface, and the second one approximately accounts for the effects of elastic wave radiation. This latter term is significant essentially during rapid slip (earthquakes).

Equations 1 to 2 and 4 to 9 are solved numerically following Dublanchet (2019) to get the pressure, slip rate, and state variable histories resulting from a particular choice of Π_m, D_0, τ_v, and initial conditions. The spatial convolution between $\mathcal{K}$ and δ is here computed in the spatial Fourier domain assuming a L-periodic slip distribution along the fault at each time step. Doing so, the fault is divided into 2,048 computational cells, so that the grid size is always smaller than the process zone size $\mu d_c/b\sigma = 3$ m (Rubin & Ampuero, 2005).

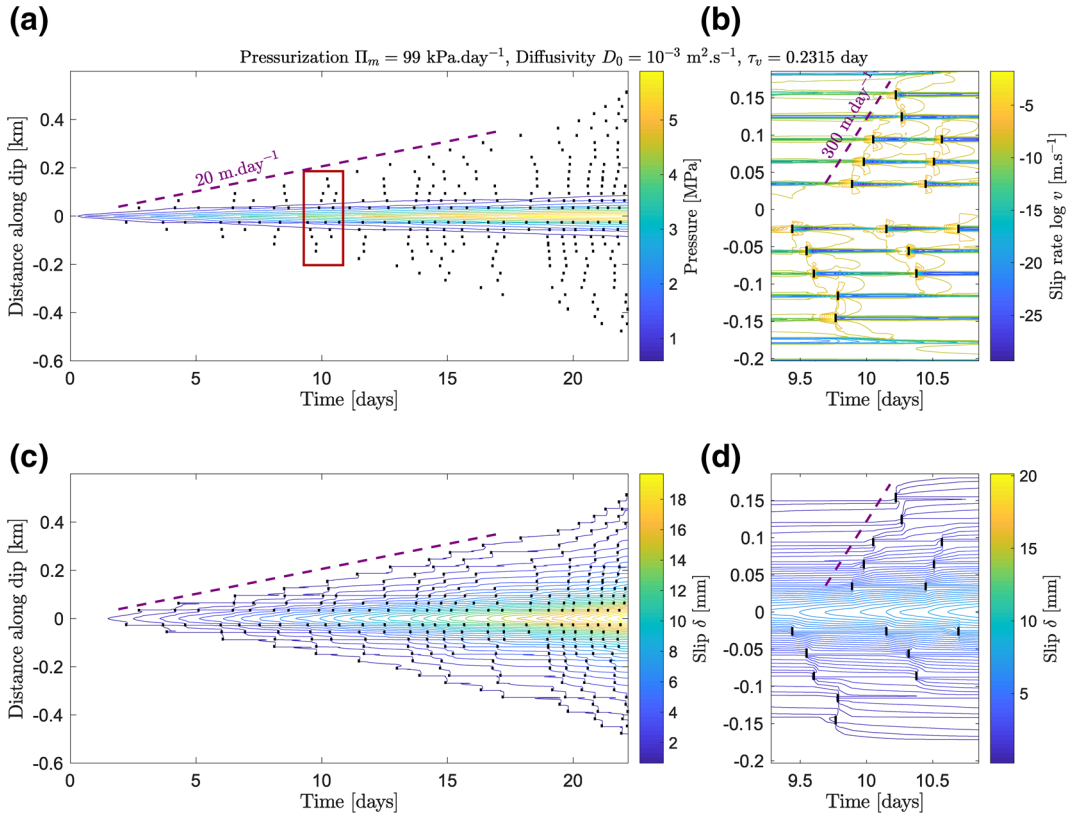

Figure 2. (a) Earthquake location versus time from injection start (black rectangles) for the simulation parameters specified in the title. Pore pressure field $p(x, t)$ is represented with colored contours. The dashed purple line indicates the global expansion of the swarm. The red box delineates the zoomed region in (b) and (d). (b) Zoom on the region outlined by the red box in (a). Black rectangles are earthquakes locations, but colored contours here refer to slip rate distribution $v(x, t)$. The dashed purple line shows a rapid migration event. (c, d) Same as (a) and (b) but with fault slip represented as colored contours.

Following Dublanchet et al. (2013), an earthquake catalog is then constructed from the slip rate history, assuming that earthquakes occur for slip rate above 1 mm s^{-1}.

3. Results

Here, we discuss the seismicity and pore pressure patterns obtained in simulations considering different mechanical and hydraulic conditions. For that we considered reference diffusivities D_0 from 9.10^{-2} to 9.10^{-7} m^2 s^{-1}. Recall that D_0 is approximately the maximum possible diffusivity one could expect during a simulation. The diffusivities considered therefore cover the range of diffusivities expected on deep faults (Doan et al., 2006; Jaeger et al., 2009) and the lower end of what is measured from seismic migration. Furthermore, we tested different values of the characteristic viscoelastic time scale: $\tau_v = \infty$ (then, the diffusivity is constant $D = D_0$), $\tau_v = 0.11$ days and $\tau_v = 0.23$ days. Finite values of τ_v correspond to effective viscosities of the order of 10^{14}–10^{15} Pa s. We also assumed pressurizations Π_m ranging from 11.5 mPa s^{-1} to 11.5 Pa s^{-1} (0.99 kPa day^{-1} to 0.99 MPa day^{-1}). Π_m is not known for natural faults, but this set of hydraulic parameters typically leads to an increase of fault pore pressure of the order of a few kPa to a few MPa over 10 days, i.e., a fraction of the lithostatic stress σ (see Figure 2 and supplementary material).

Finally, we used initial slip rate $v(x, 0)$ and state variable $\theta(x, 0)$ so that creeping areas are initially close to frictional steady state at v_0, and velocity-weakening asperities are far below steady state (they are locked). We noted that our results are not really sensitive to initial conditions on the seismogenic asperities, because as shown later the creeping sections control the triggering of seismicity. We therefore assumed different

initial conditions only on the creeping sections and defined for that the understress ratio S_0 which quantifies the distance to frictional steady state at v_0:

$$S_0 = \frac{\tau_f(x,0) - \tau_{ss}(v_0)}{\tau_{ss}(v_0)} = \frac{\tau_f(x,0) - f_0\sigma}{f_0\sigma}, \tag{10}$$

where $\tau_{ss} = f_{ss}\sigma$. Since many sources of evidence suggest that creeping faults are most of the time close to steady state (Helmstetter & Shaw, 2009), we only consider slight deviations (S_0 of a few percent). We end up with a total of 40 simulations (see Table S1 of the supplementary material for the details).

An example of synthetic seismicity is shown in Figure 2. As the injection proceeds, pore pressure diffuses along the fault, and many earthquakes are triggered (Figure 2a). The seismicity pattern consists of a swarm expanding from the injection point at a rate of approximately 20 m day^{-1} and involving sequences of rapid earthquake migration. Close to the end of the sequence (after 20 days), the swarm expansion accelerates. Other simulations shown in the supplementary material also show an acceleration of the expansion when the swarm reaches the boundaries of the fault. This is likely due to an overestimation of stress introduced by the assumption of L-periodic slip distribution (necessary to compute $\mathcal{K} * \delta$ of Equation 9 in the wavenumber domain). Rapid migration sequences generally initiate near the injection point and propagate at approximately 300 m day^{-1} (Figure 2b). Interestingly, earthquakes are triggered well beyond the pressurized area (Figure 2a). The inset of figure (b) shows that within rapid migration sequences, the failure of an asperity (earthquake) generates a propagating creep event (postseismic slip) that triggers the next asperity. Rapid migration events, and more generally the expansion of seismicity is thus driven by aseismic slip and not directly by pore pressure, which explains the wider expansion of seismicity. This is also supported by the fault slip accumulated during the swarm (Figures 2c and 2d) that does not localize on the asperities. Additional tests shown in Figure S16 indicate that rapid migration speed does not vary when changing the spacing between asperities.

Note that asperities are reactivated several times during the sequence, which could be seen as repeating earthquakes. Such repeating sequences were observed within seismic swarms (De Barros et al., 2020) and during induced seismicity (Cauchie et al., 2020).

In the following, we will make the distinction between global expansion of the swarm (occurring at 20 m day^{-1} in the example of Figure 2a) and the fast migration events (occurring at 300 m day^{-1} in the example of Figure 2b). For each simulation, we computed the global expansion speed of the swarm by fitting the envelop of the earthquake locations, before the late acceleration. Then, we computed the migration speed of rapid sequences from the distribution of $|\Delta x|/\Delta t$, Δx, and Δt being the distance and time interval separating two successive events. The estimates of the two speeds are shown in Figure 3 for our 40 simulations.

In Figure 3a, the numerical estimates are compared to the speed V_a of fluid-driven slip front on velocity-strengthening faults derived by Dublanchet (2019). We choose this estimate because both global expansion and rapid migration could be seen as the propagation of a slow slip fronts (Figures 2b, 2c, and 2d) on velocity-strengthening regions separating asperities. From Dublanchet (2019), V_a is given by

$$V_a = \frac{f_0 L \Pi_m}{2\Gamma} = \frac{f_0 L \Pi_m}{2(\tau_r - \tau_0)}, \tag{11}$$

where Γ is the stress change associated with the slipping region, i.e., the difference between the residual stress τ_r left after the slip front and the initial stress τ_0 on the fault. As we are interested in the propagation of slip on velocity-strengthening regions, this difference is positive, and a mechanism is needed to release stress within the slipping patch in order to make the aseismic slip front propagate. In the case of global expansion, this mechanism is related to pore pressure increase: since $\tau = f(\sigma - p)$, the shear strength decreases near the injection point, leading to a drop of the average shear stress within the slipping patch. The energy supplied for rapid migration is different, since it occurs outside the pressurized region. In this case, the propagation of slow slip is driven by the failure of velocity-weakening patches, which release stress. The slow slip is therefore the afterslip following the failure of asperities that migrates away from the earthquake source region and leads to successive failure of neighboring asperities. We show in the supplementary material that Γ is an aseismic fracture energy density, i.e., the energy one needs to overcome to allow the propagation of a slip front over a unit distance on a velocity-strengthening region.

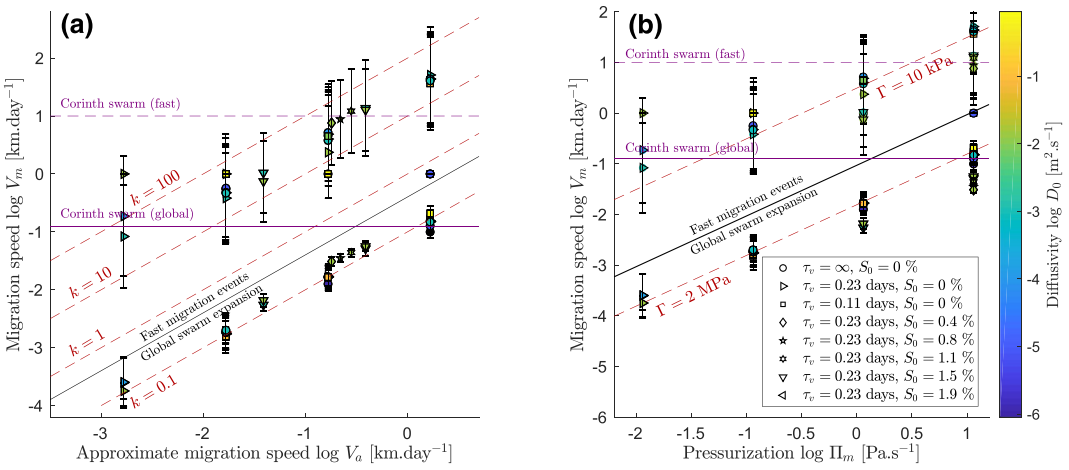

Figure 3. (a) Global expansion speeds and rapid migration speeds (V_m) estimated in the simulations (symbols) versus analytical estimates from Equation 11. The solid black line is drawn to separate global expansion and fast migration events. The approximate estimates $V_m = kV_a$ from Equation 11 are represented with dashed red lines. Solid and dashed purple lines indicate the global swarm expansion and rapid migration speeds for the Corinth swarm analyzed by De Barros et al. (2020). Symbol legend is shown in (b). The color of each symbol refers to the reference diffusivity D_0. (b) Global expansion speeds and rapid migration speeds versus pressurization Π_m (symbols). Black, red, and purple lines have the same meaning as in (a).

Note that Γ depends on S_0, and in Figure 3a, we have assumed a constant $\tau_r = 4(a-b)\sigma$ (a and b being the frictional parameters of the strengthening region) and variable τ_0 (S_0). It appears that V_a overestimates the global expansion speed by a factor of 10 and underestimates the rapid migration speeds by the same factor. It suggest that migration speeds could be written as kV_a, k being a nondimensional factor $k = 0.1$ for global expansion and $k = 20$ for rapid migration. This scaling is represented as red dashed lines in Figure 3a. We conclude that the main parameters controlling the global expansion and the rapid migration events are the pressurization Π_m and the initial state of stress on the fault. The different speeds are represented against Π_m in Figure 3b, showing a linear tendency. Here again, we compare the numerical results with the prediction of Equation 11, this time assuming constant values of Γ (accounting for the factor k). Constant Γ solutions are shown as red dashed lines in Figure 3b and provide a good estimate of our swarm expansion and fast migration speeds, with $\Gamma \simeq 2$ MPa and $\Gamma \simeq 10$ kPa, respectively.

The pressurization Π_m therefore seems to dominate over the initial state of stress in controlling the migration pattern of seismicity. However, the slope in Figure 3b is slightly different for global expansion and fast migration, suggesting that pressurization dependence is larger for global expansion speeds.

Interestingly, the hydraulic diffusivity does not significantly influence the earthquake pattern. This is the case both for the absolute value of diffusivity and for the diffusivity model (D_0 and τ_v, see also Figure S15). This could be related to the observation that earthquake triggering occurs through creep transients propagating from one asperity to another (Figures 2b, 2c, and 2d) and not by fluid flow.

In Figure 3, we also represented the estimations of global expansion speed and rapid migration speeds for the Corinth swarm analyzed in De Barros et al. (2020). These observations are compatible with a pressurization of the order of 10 Pa s^{-1} (or 0.864 MPa day^{-1}) if one assumes a lithostatic stress of the order of 150 MPa. To obtain such a pressurization, requires a pressure increase at the injection of about 12 MPa during the first day. As the expanding phase of the Corinth swarm lasts for about 5 days, the overpressure at the injection reaches 27 MPa (if we extrapolate the maximum pressure of Figure S5 using Equation 7), which is of the same order of magnitude as what is used in geothermal fields (Zang et al., 2014). Other fluid-driven swarms are characterized by migration speeds in the range 50–500 m day^{-1} (Duverger et al., 2015; Hainzl & Fischer, 2002; Hainzl et al., 2012; Goertz-Allmann et al., 2017; Lengliné et al., 2017; Shapiro & Dinske, 2009; Schoenball & Ellsworth, 2017). In light of our model, we interpret these speeds as mean pressurizations Π_m from 100 kPa day^{-1} to 1 MPa day^{-1}. Over 10 days, the overpressure at injection in such swarms is thus of the order of 0.1–10 MPa.

4. Discussion

The fault model presented here reproduces the dual migration of seismicity. We have shown that in our model, earthquake triggering is related to slow slip migration on velocity-strengthening areas. Although slow aseismic slip is triggered and sustained by the fluid injection, it expands faster along the fault than pore pressure does. Excited aseismic slip in turn triggers the failure of asperities (earthquakes) far beyond the pressurized area (Figure 2 and supplementary material). The faster expansion of slow slip front has already been reported in many modeling studies (Bhattacharya & Viesca, 2019; Cappa et al., 2018; Dublanchet, 2019; Wynants-Morel et al., 2020). Here, we show that this is even the case in the presence of seismogenic asperities.

The majority of the simulated earthquake sequences are characterized by a rather constant expansion speed. The acceleration of the expansion toward the end of the simulations is an artifact of the stress transfer computation near the fault boundaries. The expansion at constant speed is commonly observed in natural and induced sequences (De Barros et al., 2020; Lengliné et al., 2017). However, many swarms also show a diffusive pattern, i.e., with a global expansion speed decreasing as the inverse square root of time. Some simulations are characterized by diffusive expansion, where seismic activity is confined within the pressurized region, in particular for high diffusivities (see Figure S10). The transition between diffusive and linear expansion could be interpreted as differences in prestress conditions (Bhattacharya & Viesca, 2019; Wynants-Morel et al., 2020). We also observe that large understress (S_0) results in a proximity between the seismicity fronts and the pressure fronts.

The mean pressurization Π_m is the main parameter controlling the earthquake migration speeds in our simulations. Note that Π_m is not the pressure rate at the injection point $\dot{p}_0$, but the rate of increase of the spatial average of pore pressure within the fault. Π_m depends on both $\dot{p}_0$ and the effective diffusivity D (Equation 7). In the framework of induced seismicity, the injection rate could be known from borehole data, and the migration speeds could then be used to estimate at least an effective diffusivity along the activated fault.

The other parameter controlling the dynamics of such swarms is the aseismic fracture energy density Γ. Here, we have shown that global expansion and rapid migration seem to be controlled by similar physics but involving different values of Γ: the larger Γ, the smaller the migration speed. It is shown in the supplementary material that because rapid migration occurs within a region of accelerated aseismic slip (marked by the swarm extent), Γ is lowered for these rapid sequences compared to the global expansion. More generally, Γ depends on the frictional properties of the interface and in particular on the stable, velocity-strengthening properties (Dublanchet, 2019). So far, we have only considered a single distribution of the frictional properties that does not allow to better constrain Γ. This issue requires more investigation.

We have only considered a 1D fault in this study. 1D migration of seismicity is reported at the intersection of two fault systems in the Corinth area (Duverger et al., 2015), but earthquake swarm expansion is often a 2D (when a planar fault is activated), or even a 3D process (in a fault network). When considering a nonlinear diffusivity, the main difference between 1D and 2D models would come from the fluid flow, that could be channelized in 2D when asperities are locked, which is not possible in 1D. Slow slip and earthquake interaction would however obey similar processes. Studying the 3D migration requires consideration of fault networks rather than a planar fault. Fluid flow and stress transfers may in this case differ from the 1D or 2D cases. Our conclusions should therefore be restricted to the particular cases of single fault reactivation.

Driving processes of seismic swarms are often inferred from migration velocity, as slow migration velocities ($\sim$100 m s^{-1}) are associated with fluid diffusion and faster migration to slow slip (Lohman & McGuire, 2007; Vidale et al., 2006). Such velocity analysis is applied on the outermost events, but migrating sequences inside the swarms may bring new constrains on the swarm driving processes. Such dual migrations were observed in different natural swarms (Hainzl et al., 2012; Hatch et al., 2020; Hensch et al., 2008; Ruhl et al., 2016; Passarelli et al., 2018; Yoshida & Hasegawa, 2018) and reservoir stimulations (Bourouis & Bernard, 2007; Diehl et al., 2017; Eyre et al., 2019). Based on such dual migration behaviors observed in the Corinth Gulf (De Barros et al., 2020), we here propose a new model that conciliates fluid diffusion and slow slip and may successfully explain the observations of many of the swarms cited above. Even if this model may not explain all processes occurring within those swarms, it opens new interpretation possibilities and suggests that a more systematic investigation of hypocentral migration within the swarms should be performed.

5. Conclusion

We have proposed and analyzed a physics-based model for fluid-induced earthquake swarms activating a tectonic fault. The model reproduces the dual seismic migration observed in a swarm of the Corinth rift and possibly in many other fluid-induced sequences: a global expansion at 10–200 m day^{-1} of the whole swarm, involving several episodes of rapid earthquake migrations, at about 1–10 km day^{-1}. This pattern results from the coupling between fluid flow, slow slip activation, and the failure of brittle seismogenic asperities. We have shown that the fluid flow triggers expanding slow slip which promotes the repetitive failure of asperities well beyond the pressurized area. However, the main parameter controlling the migration speed is the pressurization, that is the rate of increase of the mean pore pressure within the fault, while hydraulic diffusivity plays a minor role. In our model, the pressurization required to produce the migration speeds for the Corinth swarm lead to approximately 27 MPa of overpressure at the end of the swarm. This study therefore provides a new way to interpret the hypocenter migration patterns characteristic of fluid-driven seismicity.

Data Availability Statement

Synthetic catalog of seismicity generated by the fault model is available at Dublanchet (2020).

Acknowledgments
The authors thank P. Bhattacharya, and anonymous reviewer and the associate editor for helpful comments on the manuscript.

References

Bernard, P., Lyon-Caen, H., Briole, P., Deschamps, A., Boudin, F., Makropoulos, K., & Linde, A. (2006). Seismicity, deformation and seismic hazard in the western rift of Corinth: New insights from the Corinth Rift Laboratory (CRL). *Tectonophysics*, *426*(1), 7–30. https://doi.org/10.1016/j.tecto.2006.02.012

Bhattacharya, P., & Viesca, R. C. (2019). Fluid-induced aseismic fault slip outpaces pore-fluid migration. *Science*, *364*(6439), 464–468.

Bourouis, S., & Bernard, P. (2007). Evidence for coupled seismic and aseismic fault slip during water injection in the geothermal site of Soultz (France), and implications for seismogenic transients. *Geophysical Journal International*, *169*(2), 723–732.

Bourouis, S., & Cornet, F. H. (2009). Microseismic activity and fluid fault interactions: Some results from the Corinth Rift Laboratory (CRL), Greece. *Geophysical Journal International*, *178*(1), 561–580.

Cappa, F., Guglielmi, Y., Nussbaum, C., & Birkholzer, J. (2018). On the relationship between fault permeability increases, induced stress perturbation, and the growth of aseismic slip during fluid injection. *Geophysical Research Letters*, *45*, 11012–11020. https://doi.org/10.1029/2018GL080233

Cappa, F., Scuderi, M. M., Collettini, C., Guglielmi, Y., & Avouac, J. P. (2019). Stabilization of fault slip by fluid injection in the laboratory and in situ. *Science Advances*, *5*(3), eaau4065.

Cauchie, L., Lengliné, O., & Schmittbuhl, J. (2020). Seismic asperity size evolution during fluid injection: Case study of the 1993 Soultz-sous-Forêts injection. *Geophysical Journal International*, *221*(2), 968–980.

De Barros, L., Cappa, F., Deschamps, A., & Dublanchet, P. (2020). Imbricated aseismic slip and fluid diffusion drive a seismic swarm in the Corinth gulf, Greece. *Geophysical Research Letters*, *47*, e2020GL087142. https://doi.org/10.1029/2020GL087142

Deichmann, N., & Giardini, D. (2009). Earthquakes induced by the stimulation of an enhanced geothermal system below Basel (Switzerland). *Seismological Research Letters*, *80*(5), 784–798.

Diehl, T., Kraft, T., Kissling, E., & Wiemer, S. (2017). The induced earthquake sequence related to the St. Gallen deep geothermal project (Switzerland): Fault reactivation and fluid interactions imaged by microseismicity. *Journal of Geophysical Research: Solid Earth*, *122*, 7272–7290. https://doi.org/10.1002/2017JB014473

Dieterich, J. H. (1979). Modeling of rock friction: 1. Experimental results and constitutive equations. *Journal of Geophysical Research*, *84*(B5), 2161–2168.

Dinske, C., Shapiro, S. A., & Rutledge, J. T. (2010). Interpretation of microseismicity resulting from gel and water fracturing of tight gas reservoirs. *Pure and Applied Geophysics*, *167*(1–2), 169–182.

Doan, M.-L., Brodsky, E. E., Kano, Y., & Ma, K. (2006). In situ measurement of the hydraulic diffusivity of the active Chelungpu Fault, Taiwan. *Geophysical Research Letters*, *33*, L16317. https://doi.org/10.1029/2006GL026889

Dublanchet, P. (2019). Fluid driven shear cracks on a strengthening rate-and-state frictional fault. *Journal of the Mechanics and Physics of Solids*, *132*, 103672.

Dublanchet, P.. (2020). *Synthetic earthquake catalogs generated for "Dual seismic migration velocities in seismic swarms"*. Zenodo. https://doi.org/10.5281/zenodo.3956461

Dublanchet, P., Bernard, P., & Favreau, P. (2013). Interactions and triggering in a 3-D rate-and-state asperity model. *Journal of Geophysical Research: Solid Earth*, *118*, 2225–2245. https://doi.org/10.1002/jgrb.50187

Duboeuf, L., De Barros, L., Cappa, F., Guglielmi, Y., Deschamps, A., & Seguy, S. (2017). Aseismic motions drive a sparse seismicity during fluid injections into a fractured zone in a carbonate reservoir. *Journal of Geophysical Research: Solid Earth*, *122*, 8285–8304. https://doi.org/10.1002/2017JB014535

Duverger, C., Godano, M., Bernard, P., Lyon-Caen, H., & Lambotte, S. (2015). The 2003–2004 seismic swarm in the western Corinth rift: Evidence for a multiscale pore pressure diffusion process along a permeable fault system. *Geophysical Research Letters*, *42*, 7374–7382. https://doi.org/10.1002/2015GL065298

Ellsworth, W. L. (2013). Injection-induced earthquakes. *Science*, *341*(6142).

Eyre, T. S., Eaton, D. W., Garagash, D. I., Zecevic, M., Venieri, M., Weir, R., & Lawton, D. C. (2019). The role of aseismic slip in hydraulic fracturing–induced seismicity. *Science Advances*, *5*(8), eaav7172.

Eyre, T. S., Zecevic, M., Salvage, R. O., & Eaton, D. W. (2020). A long-lived swarm of hydraulic fracturing-induced seismicity provides evidence for aseismic slip. *Bulletin of the Seismological Society of America*, *110*, 2205–2215.

Goertz-Allmann, B., Gibbons, S., Oye, V., Bauer, R., & Will, R. (2017). Characterization of induced seismicity patterns derived from internal structure in event clusters. *Journal of Geophysical Research: Solid Earth*, *122*, 3875–3894. https://doi.org/10.1002/2016JB013731

Guglielmi, Y., Cappa, F., Avouac, J.-P., Henry, P., & Elsworth, D. (2015). Seismicity triggered by fluid injection–induced aseismic slip. *Science*, *348*(6240), 1224–1226.

Hainzl, S., & Fischer, T. (2002). Indications for a successively triggered rupture growth underlying the 2000 earthquake swarm in Vogtland/NW Bohemia. *Journal of Geophysical Research*, *107*(B12), 2338. https://doi.org/10.1029/2002JB001865

Hainzl, S., Fischer, T., & Dahm, T. (2012). Seismicity-based estimation of the driving fluid pressure in the case of swarm activity in Western Bohemia. *Geophysical Journal International*, *191*(1), 271–281.

Hatch, R. L., Abercrombie, R. E., Ruhl, C. J., & Smith, K. D. (2020). Evidence of aseismic and fluid-driven processes in a small complex seismic swarm near Virginia City, Nevada. *Geophysical Research Letters*, *47*, e2019GL085477. https://doi.org/10.1029/2019GL085477

Helmstetter, A., & Shaw, B. E. (2009). Afterslip and aftershocks in the rate-and-state friction law. *Journal of Geophysical Research*, *114*, B01308. https://doi.org/10.1029/2007JB005077

Hensch, M., Riedel, C., Reinhardt, J., Dahm, T., & The, N. (2008). Hypocenter migration of fluid-induced earthquake swarms in the Tjörnes fracture zone (North Iceland). *Tectonophysics*, *447*(1–4), 80–94.

Horowitz, F. G., & Ruina, A. (1989). Slip patterns in a spatially homogeneous fault model. *Journal of Geophysical Research*, *94*(B8), 10279–10298.

Jaeger, J. C., Cook, N. G., & Zimmerman, R. (2009). *Fundamentals of rock mechanics* (4th ed.). Oxford: John Wiley & Sons.

Lengliné, O., Boubacar, M., & Schmittbuhl, J. (2017). Seismicity related to the hydraulic stimulation of GRT1, Rittershoffen, France. *Geophysical Journal International*, *208*(3), 1704–1715.

Lohman, R., & McGuire, J. (2007). Earthquake swarms driven by aseismic creep in the Salton Trough, California. *Journal of Geophysical Research*, *112*, B04405. https://doi.org/10.1029/2006JB004596

Marone, C. (1998). Laboratory-derived friction laws and their application to seismic faulting. *Annual Review of Earth and Planetary Sciences*, *26*(1), 643–696.

Obara, K. (2010). Phenomenology of deep slow earthquake family in southwest Japan: Spatiotemporal characteristics and segmentation. *Journal of Geophysical Research*, *115*, B00A25. https://doi.org/10.1029/2008JB006048

Passarelli, L., Rivalta, E., Jónsson, S., Hensch, M., Metzger, S., Jakobsdóttir, S. S., & Dahm, T. (2018). Scaling and spatial complementarity of tectonic earthquake swarms. *Earth and Planetary Science Letters*, *482*, 62–70.

Radiguet, M., Cotton, F., Vergnolle, M., Campillo, M., Valette, B., Kostoglodov, V., & Cotte, N. (2011). Spatial and temporal evolution of a long term slow slip event: The 2006 Guerrero slow slip event. *Geophysical Journal International*, *184*(2), 816–828.

Rice, J. R. (1993). Spatio-temporal complexity of slip on a fault. *Journal of Geophysical Research*, *98*(B6), 9885–9907.

Rubin, A. M., & Ampuero, J.-P. (2005). Earthquake nucleation on (aging) rate and state faults. *Journal of Geophysical Research*, *110*, B11312. https://doi.org/10.1029/2005JB003686

Rubin, A. M., & Armbruster, J. G. (2013). Imaging slow slip fronts in Cascadia with high precision cross-station tremor locations. *Geochemistry, Geophysics, Geosystems*, *14*, 5371–5392. https://doi.org/10.1002/2013GC005031

Ruhl, C., Abercrombie, R., Smith, K., & Zaliapin, I. (2016). Complex spatiotemporal evolution of the 2008 M_w 4.9 Mogul earthquake swarm (Reno, Nevada): Interplay of fluid and faulting. *Journal of Geophysical Research: Solid Earth*, *121*, 8196–8216. https://doi.org/10.1002/2016JB013399

Ruina, A. L. (1983). Slip instability and state variable friction laws. *Journal of Geophysical Research*, *88*(B12), 10359–10370.

Schoenball, M., & Ellsworth, W. L. (2017). A systematic assessment of the spatiotemporal evolution of fault activation through induced seismicity in Oklahoma and southern Kansas. *Journal of Geophysical Research: Solid Earth*, *122*, 10–189. https://doi.org/10.1002/2017JB014850

Shapiro, S. A., & Dinske, C. (2009). Scaling of seismicity induced by nonlinear fluid–rock interaction. *Journal of Geophysical Research*, *114*, B09307. https://doi.org/10.1029/2008JB006145

Vidale, J. E., Boyle, K. L., & Shearer, P. M. (2006). Crustal earthquake bursts in California and Japan: Their patterns and relation to volcanoes. *Geophysical Research Letters*, *33*, L20313. https://doi.org/10.1029/2006GL027723

Wei, S., Avouac, J.-P., Hudnut, K. W., Donnellan, A., Parker, J. W., & Graves, R. W., et al. (2015). The 2012 Brawley swarm triggered by injection-induced aseismic slip. *Earth and Planetary Science Letters*, *422*, 115–125.

Wynants-Morel, N., Cappa, F., De Barros, L., & Ampuero, J. P. (2020). Stress perturbation from aseismic slip drives the seismic front during fluid injection in a permeable fault. *Journal of Geophysical Research: Solid Earth*, *125*, e2019JB019179. https://doi.org/10.1029/2019JB019179

Yoshida, K., & Hasegawa, A. (2018). Sendai-Okura earthquake swarm induced by the 2011 Tohoku-Oki earthquake in the stress shadow of NE Japan: Detailed fault structure and hypocenter migration. *Tectonophysics*, *733*, 132–147.

Zang, A., Oye, V., Jousset, P., Deichmann, N., Gritto, R., McGarr, A., & Bruhn, D. (2014). Analysis of induced seismicity in geothermal reservoirs–an overview. *Geothermics*, *52*, 6–21.

References From the Supporting Information

Dieterich, J. H., & Kilgore, B. D. (1994). Direct observation of frictional contacts: New insights for state-dependent properties. *Pure and Applied Geophysics*, *143*(1–3), 283–302.

Lawn, B. (1993). *Fracture of brittle solids* (p. 208). Cambridge University Press.

Witherspoon, P. A., Wang, J. S., Iwai, K., & Gale, J. E. (1980). Validity of cubic law for fluid ow in a deformable rock fracture. *Water Resources Research*, *16*(6), 1016–1024.